Geochimica et Cosmochimica Acta 0016-7037/78/0615-0725$02.00/0
Vol. 42, pp. 725-741

MODELLING OF MAJOR ELEMENTS IN MANTLE-MELT SYSTEMS USING TRACE ELEMENT APPROACHES

Gilbert N. Hanson and Charles H. Langmuir

Department of Earth and Space Sciences
State University of New York
Stony Brook, New York 11794

ABSTRACT

Major elements can be modelled in ways similar to the quantitative petrogenetic modelling used for trace elements. In contrast to modelling with trace elements, however, modelling with major elements is constrained by the stoichiometry of the solid phases. Within these constraints, the same equations for partial melting and crystallization which have been used to such advantage for trace elements may be used for major elements.

Calculated MgO and FeO abundances in a mantle-melt system are used as an example of the modelling technique. Such modelling yields limited fields of permissible melts and residues for a given parent composition, but does not give the paths of melting. It does allow the temperature and extent of melting which gave rise to a melt to be determined from the MgO and FeO abundances of the melt or residual solid. Applying the results of the modelling to igneous rocks and ultramafic nodules leads to the following conclusions, which are subject to the uncertainties in the available distribution coefficients. Least differentiated basalt glasses from the ocean floor are derived from parent melts with less than 15.5 weight % MgO and 8.2 wt. % FeO. Komatiites may be derived by less than 60% melting of a pyrolite source leaving a residue of olivine and pyroxene. Many nodules from the subcontinental mantle appear to be residues of large fractions of melting (>30%) at high temperature and pressure, whereas ultramafic nodules from oceanic basalts appear to be residues of smaller fractions of melting (<30%) at lower temperatures and pressures.

INTRODUCTION

In petrogenetic studies of igneous rocks, major and trace elements have generally been treated in different ways. Although major elements have been extensively used, they have not received the quantitative treatment which has proven so valuable for trace elements.

The different approaches towards major and trace elements have been based on the distinction between elements which follow Henry's Law (trace elements) and those which make up significant proportions of the sites in the phases considered. The breakthrough for modelling with trace elements occurred with the recognition that the distribution of a single trace element between mineral and melt phases could be represented by a distribution coefficient (K_d) over a range of abundances in the phases involved. This led to the development of equations describing the distribution of trace elements during partial melting and crystallization (e.g. NEUMANN et al., 1954; SCHILLING, 1966; GAST, 1968; SHAW, 1970; etc.).

The distribution of major elements during partial melting and crystallization has been dealt with from other points of view making use of exchange reaction distribution coefficients (K_D), phase diagrams and unmixing of phases during fractional crystallization. For example, PRESNALL (1969) showed how phase diagrams could be used to understand the processes of partial fusion. MORSE (1976) demonstrated how to extract quantitative information from phase diagrams and dealt with the relationship between phase diagrams, the distribution coefficient (K_d) and the Rayleigh fractionation law. Both these workers dealt with simple systems which had been well studied experimentally. ROEDER (1975) showed how to model fractional crystallization of olivine and plagioclase in

real systems using the exchange reaction distribution coefficient, K_D. IRVINE (1974) has also worked extensively with modelling major elements, particularly during crystallization, using both phase diagrams and the exchange reaction distribution coefficient. WRIGHT and DOHERTY (1970) described an unmixing method to show how melts evolve during fractional crystallization.

In this paper, major elements are approached from the trace element point of view ulitizing mineral-melt distribution coefficients (K_d's) for individual elements in real systems. We suggest that: (1) major and trace elements need not be considered separately and that they belong to a continuum of chemical behavior involving the type of solution and degree of stoichiometric constraint on an element's behavior; (2) within these constraints, the mineral-melt distribution coefficient (K_d) for a single element is equally useful for major as well as trace elements; and (3) the same quantitative methods which have been applied to modelling trace element abundances may be applied to major elements. Symbols and terms used in this paper are defined in Table 1.

Theory

The theoretical basis for the quantitative treatment of trace elements in igneous rocks relies on the distribution law,

$$K_d = C_\alpha/C_L \quad (a) \qquad D = \sum X K_d = C_s/C_L \quad (b) \qquad (1)$$

where C_α is the concentration of the element in a mineral, C_s is the concentration of the element in the total solid, C_L is the concentration of the element in the melt, X is the fraction of the mineral in the residue, and D is the bulk distribution coefficient for a group of minerals.

During batch melting, simple mass balance requires that

$$C_O = FC_L + (1-F)C_s \qquad (2)$$

where F is the fraction of melting and C_O is the initial concentration of the element. This equation is also the lever rule used with phase diagrams. For those elements for which the distribution law holds, SCHILLING (1966) showed that substituting for C_s from equation 1(b) yields what is referred to as the batch melting equation for trace elements.

$$C_L/C_O = 1/(D(1-F) + F) \qquad (3)$$

Table 1. Definition of symbols and terms used

C_o^i	- Concentration of a given element, i, in the total system considered at the time a given process begins.
C_L^i	- Concentration of a given element, i, in the melt.
C_s^i	- Concentration of a given element, i, in the solid phases.
C_{ol}^i	- Concentration of a given element, i, in olivine.
C_α^i	- Concentration of a given element, i, in a mineral.
F	- The fraction of melt relative to the original system.
$K_{d_i}^{\alpha/L}$	- The mineral (α)-melt (L) distribution coefficient for a given element or oxide, i. It may be expressed in either mole or weight fractions. $K_{d_i}^{\alpha/L} = C_\alpha^i/C_1^i$
K_D	- The exchange reaction distribution coefficient. It is the ratio of K_d's for two different elements for the same phases.
X^α	- The mole or weight fraction of a given mineral, α, in the solid phases.

D_i - The bulk solid-melt distribution coefficient for a given element or oxide at the time of removal of the melt from the solid phases. It may be expressed in terms of mole or weight fractions.

$$D_i = \sum_i X^{\alpha} K_{d_i}^{\alpha/L}$$

Fractional Crystallization - The instantaneous equilibrium precipitation of an infinitismally small amount of crystals which are then completely removed from the system (BOWEN, 1928).

Batch Melting or Equilibrium Fusion (PRESNALL, 1969) - Melting in which after a certain fraction of melting, the melt is removed from the solid phases and there is no further melting.

Fractional Melting of Fractional Fusion - Melting in which fractions of melt are continuously and completely removed from the solid phases as melting proceeds (BOWEN, 1928; PRESNALL, 1969).

Continuous Melting - Melting in which fractions of melt are continuously, but not completely removed from the solid phases as melting proceeds (LANGMUIR et al., 1977; LANGMUIR and HANSON, 1975).

For fractional crystallization, elements for which the distribution law applies follow the Rayleigh fractionation law (NEUMANN et al., 1954)

$$C_L/C_O = F^{(D-1)} \qquad (4)$$

where F in this case is the fraction of melt remaining. These equations, and their many refinements, should be valid for any element in a mineral-melt system for which a K_d can be defined. Since a K_d can be defined for both major and trace elements, the so-called "trace element equations" may, with certain restrictions, also be applied to major elements.

Definitions of Three Types of Elements in Mineral-Melt Systems

The essential distinction between trace elements and major elements when considering their distribution between solid and liquid phases is that the abundance of a trace element in a mineral is so small that it is not constrained stoichiometrically, but is simply related by a K_d to the concentration of the element in the liquid. Major elements, however, are constrained to a definite range in abundances in a liquid for a given K_d by the stoichiometry of the minerals present in the system. For example, if the K_d for MgO between olivine and liquid is 10, MgO in the liquid would be constrained to less than 6.67 mole %, because MgO in olivine is constrainted to less than 66.7%.

Extreme cases of stoichiometric constraints apply to elements which are essential structural constituents (ESC's) in minerals (SUN and HANSON, 1975). An ESC is an element which completely fills one site in a mineral and for which there is very little solid solution. For example, K in phlogopite would be an ESC if the substitution of other elements for K were small. Since K has a fixed abundance in phlogopite, the concentration of K in the melt would be a direct function of the K_d, as long as phlogopite was a solid phase in the system. In contrast to trace elements, the concentration of K in the melt could change only if K_d changed, and would be independent of the fraction of phlogopite in the total solid.

The presence or absence of stoichiometric constraints and the type of solid solution lead to the following definitions of elements (Figure 1):

A trace element is an element whose concentration is so low that there is no stoichiometric constraint on its abundance in minerals or liquids. For a given K_d, the trace element may have a wide range of abundances in both minerals and liquids. A trace element in an ideal solution, follows Henry's Law or the activity coefficients covary systematically in the phases involved.

An essential structural constituent (ESC) is an element which totally fills a site in any mineral in the system. For a given K_d, an ESC has a fixed abundance in the liquid in equilibrium with the mineral. For limited solid solution the ESC will follow Raoult's Law.

An intermediate element lies between these two end members. For a given K_d, the abundance of the element in both mineral and liquid can vary, but only within the limits imposed by stoichiometry. For intermediate elements solid solution may follow Raoult's or Henry's Law, or be ideal or non-ideal. For non-ideal solutions, an intermediate element may be of low enough abundance in a mineral that it is not constrained stoichiometrically, yet it may not fulfill the solution criteria for trace elements. For such an element, K_d will vary as the abundance of the element varies.

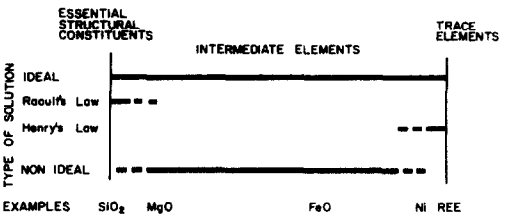

Figure 1. Illustration of the classification of elements in mineral-melt systems as a function of the type of solid solution and extent of stoichiometric control. The stoichiometric constraints decrease from essential structural constituents to trace elements. SiO_2, MgO, FeO, Ni and REE in a forsterite-rich, olivine-melt system are shown as examples.

When they are viewed in this way, all elements in mineral-melt systems are part of a continuous series between ESC's and trace elements. The two end-members are approached but not reached, since every mineral site shows some substitution and trace elements in one system may be abundant enough in another system to be important to mineral structures.

It is in this context of element behavior that the equations for partial melting and crystallization can be used. The equations serve no useful purpose for ESC's because K_d immediately specifies the liquid composition with no further calculation. For trace elements, the equations describe how an element's abundance will change as a function of the degree of melting or crystallization. For intermediate elements, the equations give the same information as for trace elements, except that the compositions of the minerals in the residue must be continuously monitored during modelling to ensure that no stoichiometric violations occur.

MODELLING OF MgO AND FeO

In the following sections, as examples of modelling major elements with K_d's, we will model the MgO and FeO abundances in melts and residual solids derived by partial melting of pyrolite (RINGWOOD, 1975), and in melts undergoing fractional crystallization of olivine from any melt in equilibrium with olivine.

From the outset it should be realized that we cannot determine the unique path of melting for a parent composition. We can, however, determine the field of permissible melts which are consistent with the mineralogy and the available K_d's. For fractional crystallization, it is possible to calculate the path of the melt if olivine were crystallizing.

Calculation of the MgO and FeO Abundances for Partial Melting of the Mantle

For modelling of MgO and FeO during partial melting of the mantle, it would be ideal to know K_d's for all mantle minerals as well as how the mineral proportions change with extent of partial melting in order to calculate the D's. Even though these data are not available, it is still possible to model MgO and FeO accurately because of the following relation for D:

$$D = \frac{C_s}{C_L} = \frac{C_s}{C_{ol}} \frac{C_{ol}}{C_L} = \frac{C_s}{C_{ol}} K_d^{ol/L} \qquad (5)$$

Thus, for any mineralogy and bulk composition, D for MgO and FeO can be determined if we know the concentration of these elements in the residue and their concentration in the olivine in that residue. Inspection of abundant analyses of MgO and FeO for minerals in ultramafic nodules reveals that the olivine/orthopyroxene K_d's for MgO and FeO are essentially constant. The preponderance of olivine and orthopyroxene in the mantle allows an estimation of the olivine composition to with $\pm$ $Fo_{0.5}$, even though olivine/clinopyroxene and olivine/garnet K_d's for MgO and FeO vary with T and P (e.g. see RÄHEIM and GREEN, 1976).

To demonstrate the method, we will use the following equations at one atmosphere (ROEDER and EMSLIE, 1970) for the variation of olivine/melt K_d's with temperature for MgO and FeO:

$$\log_{10} K_{d_{MgO}} = \frac{3740}{T} - 1.87 \qquad (6)$$

$$\log_{10} K_{d_{FeO}} = \frac{3911}{T} - 2.50 \qquad (7)$$

In using this technique for a given suite of rocks, it would be necessary to know the temperature, pressure, and composition dependence of the K_d's for the suite. The above relations are typical for low K tholeiites at one atmosphere and temperatures of 1000-1300°C (ROEDER and EMSLIE, 1970; ROEDER, 1974).

For a given mantle composition and temperature, MgO and FeO distributions in solids and liquids are first calculated for minimum (F=0) and maximum extents of melting. For the composition of the initial melt (F=0), D is given by equation (5) where C_s is the original composition of the mantle (i.e. $C_s = C_o$), in this case pyrolite, and the olivine composition is estimated for the initial mantle composition (for pyrolite this is $Fo_{89.5}$). For F=0 equation (3) when combined with equation (5) becomes

$$C_L = \frac{C_o}{D} = \frac{C_{ol}}{K_d^{ol/L}} \qquad (8)$$

This relation allows a unique liquid composition to be calculated for each temperature.

The maximum extent of permissible melting at a given temperature occurs when olivine is the only residual phase. Then $D = K_d^{ol}/L$ and

$$C_L = \frac{C_o}{K_d\ (1-F) + F} \qquad (9)$$

$$C_s = C_L\ K_d \qquad (10)$$

There are two such equations for MgO and FeO, and there is the additional equation relating the molar concentration of MgO and FeO in olivine:

$$MgO + FeO = 66.67\% \qquad (11)$$

These five equations relate the five unknowns: F and the abundances of MgO and FeO in the liquid and solid. The calculation of the maximum extent of partial melting is not dependent on estimating the olivine composition, and the unknowns can be uniquely determined. When these calculations for minimum and maximum extents of partial melting are carried out over a range of temperatures, fields of permissible melts and residual solids from a given initial composition are given (Figure 2).

Calculating the MgO and FeO distributions for F between maximum and minimum extents of melting is slightly more complicated. For a given F, there are eight equations and eight unknowns, so a solution is possible. The eight equations are (1a), (3), and (5) for MgO and FeO, equation (11) and the estimated relation between the total composition of the residue and olivine in the residue based on the mineral compositions in ultramafic nodules. The eight unknowns are the MgO and FeO compositions of the residue, olivine and melt and the D's for MgO and FeO.

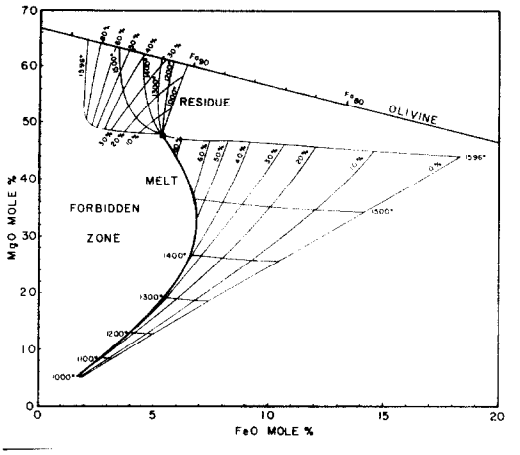

Figure 2. MgO-FeO diagram for the pyrolite-melt system at one atmosphere showing the compositions of pyrolite (solid square) and olivine, and the fields for melts and residues for batch melting. The temperature and fraction of melting are contoured in both fields.

For the designated F, a D is selected intermediate between that for minimum and maximum melting, and C_L (the melt) and C_S (the residue) are calculated for both MgO and FeO using equations (1b) and (3). The composition of the olivine is then estimated for that residue. Using this olivine composition, new D's are calculated using equation (5). These D's are then used in equations (1b) and (3) and the process is repeated until the melt, residue, and olivine are compatible with one another. Usually two or three iterations are sufficient for convergence within 1%. A numerical example of a calculation is given in appendix 1.

For any of the calculations, MgO and FeO cannot be calculated separately because the number of unknowns would then exceed the number of equations. The stoichiometric constraints on MgO and FeO in olivine require knowledge of the residual olivine composition, but allow determination of the change in MgO and FeO abundances as a function of the degree of partial melting without any assumptions about how the mineral proportions in the source are changing. Furthermore, the stoichiometric constraints allow a determination of the maximum permissible extent of melting for a given temperature and bulk composition. Thus, more information is needed to model the major elements, but there is a compensating increase in information obtained.

The stoichiometric constraints for major elements prohibit simple use of the batch melting equation to calculate C_L given simple C_o, D and F (as is done for trace elements), because the melt must always be in equilibrium with real (stoichiometric) minerals. The validity of any melting calculation may be checked by calculating the compositions of the residual minerals to make sure they are stoichiometrically valid.

The MgO-FeO Diagram for Partial Melting

Figure 2 shows graphically the results for the batch melting of pyrolite (RINGWOOD, 1975) using the K_d data of ROEDER and EMSLIE (1970). There are two fields, one for melts and the other for residual solids, each with contours of temperature and percent melting. The melt field is bounded on the right by the 0% melting line. It is bounded on the left by the line where olivine is the only mineral in the residue at various temperatures. This corresponds to the upper bound of the residue field, which is the line of olivine composition. The upper bound of the melt field occurs at the temperature which intersects the parent composition. This temperature is the liquidus temperature of the parent, provided that the K_d's are correct. Extrapolating the K_d's of ROEDER and EMSLIE (1970), which were measured up to 1300°C, the liquidus temperature of pyrolite at one atmosphere would be 1596°C.

Although the diagram gives a melting field and not a unique path of melting (which would be a line on the diagram), this does not restrict its usefulness. When a rock which once was a primary melt is plotted in this field, its position gives information on the temperature and the extent of melting which led to the formation of the melt, assuming a parent composition and provided that the K_d's are appropriate.

When a suite of rocks are plotted, they may give information about the path of melting. The actual path of melting need not be similar to those determined by experiments at one pressure and various temperatures such as the experiments of MYSEN and KUSHIRO (1977). Among other things, the path of melting depends on the pressure at which melting takes place, the concentration of volatiles, and whether melting occurs in a rising diapir or a static mantle to which volatiles or heat are added. For example, if melting occurs in a diapir rising adiabatically, progressive melting may be associated with decreasing temperature and pressure.

Although the diagram as shown in Figure 2 is strictly valid only for one parent composition at low pressures and uses extrapolated data for temperatures above 1300°C, the following features of the diagram should be generally valid:

(1) For a given set of K_d's, the melt field is tied to the isotherms, which are the same as those on the olivine saturation surface of ROEDER and EMSLIE (1970). The extent of melting increases with a slight increase in MgO and a larger decrease in FeO for each isotherm. Because the isotherms are fixed in position, changing the MgO content of the parent has little or no effect on the MgO content of the derived melts for a given temperature as long as olivine is in the residue. Changing the FeO content of the parent simply moves the partial melting field along the isotherms to higher or lower FeO abundances.

(2) The isotherms are straight lines with slopes equal to $-K_D$. Even if K_D varies with temperature and pressure, the variation will probably not be large enough to change appreciably the slope of the isotherms and hence the shape of the partial melting field. So the general configuration shown in Figure 2 is probably valid for a wide range of temperatures, pressures, and parent compositions.

The general configuration of the diagram permits certain generalizations about the MgO and FeO concentration of liquids generated by partial melting of the mantle. The atomic ratio of $Mg/(Mg + Fe^{2+})$ or Mg# can vary widely in primary liquids, and is a function of the temperature and extent of melting. For example, a very low percentage melt at 1400°C would have an Mg# of about 0.72, while a 30% melt would have an Mg# close to 0.80. Higher temperature melts have a higher Mg# for a given percentage of melting than lower temperature melts. The residual mineralogy is dependent on both the fraction of melting and the temperature at which melting occurs. For example, if the path of melting led to 40% melting at 1400°C, olivine would be alone in the residue. If instead 40% melting occurred at 1500°C, other minerals would be present in the residue with olivine.

Effect of Continuous Melting

Batch melting, for which the fields in Figure 2 are constructed, is only one possible model. In batch melting there is no further melting after the melt is removed from contact with the residue. At the other extreme is fractional

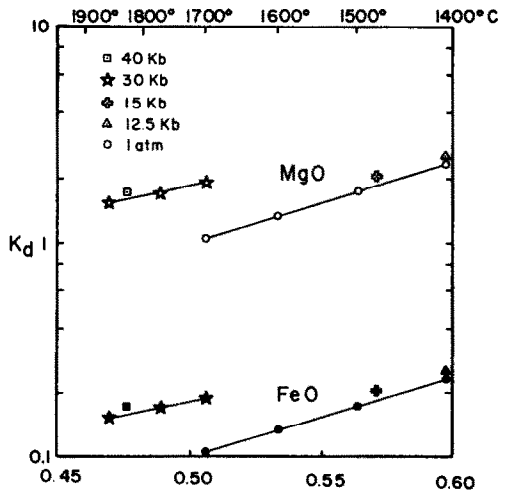

Figure 3. Plot of K_d vs. 1/T for FeO and MgO in olivines and melts at various pressures. The one atmosphere data are extrapolated using the regression equations of ROEDER and EMSLIE (1970). Other data are from LONGHI et al., (in press) and BICKLE et al. (1977).

fusion where a fraction of melt is continuously and completely removed from contact with the residual solids as melting proceeds. Continuous melting (LANGMUIR et al., 1977; LANGMUIR and HANSON, 1977) is an intermediate process where melt is continuously but not completely removed, so a portion of the melt remains behind in the residue.

During batch melting, the bulk composition of the system remains unchanged until melting is completed. For continuous melting, the bulk composition of that part of the system where melting is occurring is changing continuously as melt is removed. This makes the "parent" for later melts progressively more refractory and depleted in the less compatible trace elements, i.e. those elements for which D is less than one.

For continuous melting, the 0% melting line of the partial melting field remains the same. At temperatures greater than 1300°C, where the K_d for FeO is less than one, lines of higher extents of partial melting are moved toward lower FeO abundances because the bulk composition of the effective parent is moving to lower FeO and higher MgO abundances as melting proceeds. At temperatures less than 1300°C, the parent moves toward higher FeO and MgO abundances. Continuous melting thus provides a way, at temperatures greater than 1300°C, of crossing the maximum partial melting line for batch melting and entering the forbidden zone. At 1525°C, a total melting of 25% fractional fusion of a pyrolite mantle gives the same MgO and FeO abundances in a melt as 60% batch melting. Thus melts which plotted at that particular point in the MgO-FeO plot could be derived from anywhere between 25 and 60% melting depending on whether continuous or batch melting was taking place.

The Effect of Pressure on the MgO-FeO Diagram

The K_d's for MgO and FeO used in Figure 2 (ROEDER and EMSLIE, 1970) were determined at one atmosphere. In order to consider melting at higher pressures it would be necessary to know the K_d's at the higher pressures, and to calculate the effect on the MgO-FeO diagram. One known effect is that at higher pressures the liquidus temperature of the mantle must be greater than at one atmosphere. The liquidus temperature of the mantle, the upper bound of the melt field, is a straight line which passes through the parent composition and has a slope of $-K_D$. Although the slope of this line may change with increased pressure, this isothermal line must always pass through the parent composition. Thus, increasing pressure increases the temperature for this isothermal line and would suggest that all the isotherms on the MgO-FeO plot are displaced to lower MgO values at higher pressures. To lower the isotherms requires increased K_d's for MgO, which suggests that the K_d's for MgO at a given temperature increase with increasing pressure.

The available experimental data are consistent with this reasoning. Figure 3 presents data for MgO and FeO at one atmosphere (ROEDER and EMSLIE, 1970), 12.5 Kb (LONGHI et al., in press), 15 Kb, 30 Kb and 40 Kb (BICKLE et al., 1977). The data for both MgO and FeO show a gradual increase in K_d with pressure at a given temperature. K_D appears to also increase slightly with pressure. Figure 4 shows the melt and residual solid fields calculated for the K_d's at 30 Kb on the MgO-FeO diagram shown in Figure 2. The striking feature is that the fields at 30 Kb are similar to the fields at one atmosphere, except that the temperatures are higher. Thus until more data become available, the one atmosphere data may be a reasonable approximation for extents of partial melting at low or high pressures.

The high pressure experimental data also allow an estimate to be made of the relative position of the solidus as a function of pressure. Based on the high pressure data in Figure 3, the isothermal lines are lowered approximately 4-8°/Kb on the MgO-FeO plot. According to GREEN (1976), the pyrolite solidus increases approximately 10°/Kb. For a fixed volatile content, the position of the solidus along the 0% melting line will increase about 5°/Kb with respect to the one atmosphere isotherms, and liquids derived by small degrees of partial melting will move towards increasing MgO and FeO content with increasing pressure. Thus, potentially the MgO and FeO concentrations of primary melts can be used to tell the pressure at which the melts formed.

Figure 4. MgO-FeO diagram for bath melting of pyrolite. The shaded fields show the results for K_d data measured at 30 Kb (BICKLE et al., 1977) which can be compared to the results for K_d data measured at one atmosphere (ROEDER and EMSLIE, 1970) in the unshaded fields.

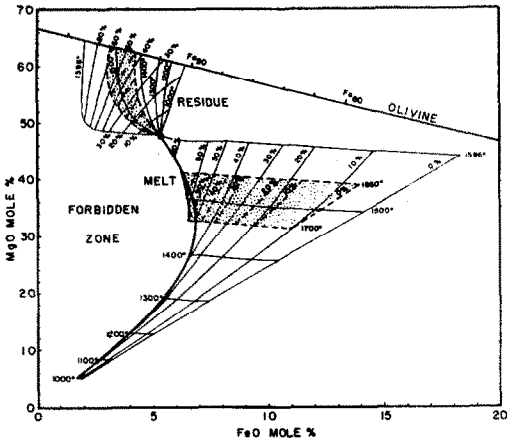

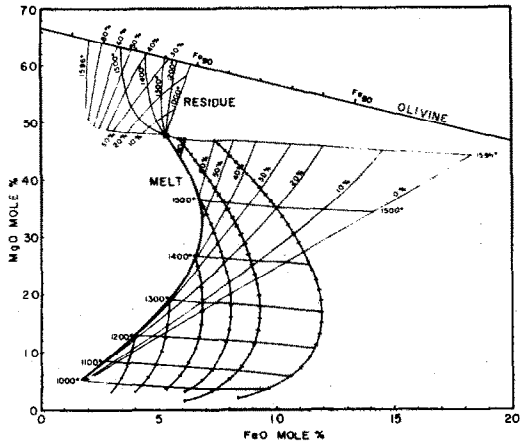

Figure 5. MgO-FeO diagram for batch melting of pyrolite from Figure 2 with curves for fractional crystallization of olivine from melts at one atmosphere. The marks along the curves are at intervals of 5% fractional crystallization of olivine and are applicable starting at any position along a curve.

MgO-FeO Distributions During Fractional Crystallization of Olivine

Abundances of MgO and FeO during fractional crystallization of olivine can be modelled using the K_d's and equation 4. Fractional crystallization has been modelled in slightly different ways by ROEDER (1975) and IRVINE (1974). As with partial melting, the stoichiometric constraints required that MgO and FeO be modelled together. 0.1% olivine is fractionally crystallized using equation (4) with the appropriate K_d's for MgO and FeO from equations (6) and (7). The residual olivine composition for the new melt is calculated using the original K_d's. This residual composition will not have the proper MgO and FeO contents to make olivine, so it is necessary to proportionally change the MgO and FeO contents of the olivine by renormalizing the sum of the FeO plus MgO concentration to 66.67% (in olivine, SiO_2 is 33.33 mole%). A new K_d is calculated for both MgO and FeO based on this olivine composition and the melt composition. A further 0.1% fractional crystallization is then calculated using equation (4). At each new step, a temperature can be calculated from equations (6) and (7) using the K_d's calculated at each step. This way of modelling differentiation is fundamentally different from subtracting average phenocryst compositions from a liquid composition, because it accounts for the change of olivine composition with change of liquid composition. This calculation does not predict whether olivine is crystallizing. It only shows the path of the melt in the MgO-FeO diagram if olivine were fractionally crystallizing.

In Figure 5 are plotted lines for fractional crystallization of olivine with 5% increments of fractional crystallization marked off. The tangent to the curve at a given melt composition intersects the composition of the olivine crystallizing. The subparallel nature of the curves allow an estimate of the

effect of the fractional crystallization of olivine from any melt. At temperatures greater than 1300°C, where the K_d for Fe is less than one, FeO is enriched in the melt while MgO is depleted. At temperatures less than 1300°C both MgO and FeO are depleted in the melt. Only at temperatures less than 1100°C is the depletion of FeO severe.

For melts which are in equilibrium with olivine at a given pressure, crystallization of minerals which gives the melt a higher MgO content is not allowed, since this would require raising the temperature of the melt. Crystallization of plagioclase, orthopyroxene, clinopyroxene, and probably garnet all drive melts to higher FeO content than does olivine. This means that any given melt which has undergone subtraction of these phases must come from a primary magma which is less iron rich than the olivine fractionation lines through the point where the derivative magma plots on the MgO-FeO diagram. The only phases to cause depletion in Fe would be the oxides.

TRACE ELEMENTS

This section examines how the abundances of trace elements vary in comparison to the abundances of major elements. For melts derived by partial melting of pyrolite, the abundances of MgO will be compared with those of Ni (a compatible element) and with those of incompatible elements, for which D is effectively zero.

The MgO-Ni Diagram

Figure 6 shows MgO in mole% plotted against Ni in ppm for melts and residues derived by batch melting of a pyrolite mantle with 1800 ppm Ni. Fields for melting at one atmosphere and 30 Kb are shown. Also plotted are curves for the fractional crystallization of olivine at one atmosphere. K_d's at one atmosphere for MgO are from ROEDER and EMSLIE (1970) and at 30 Kb are from BICKLE

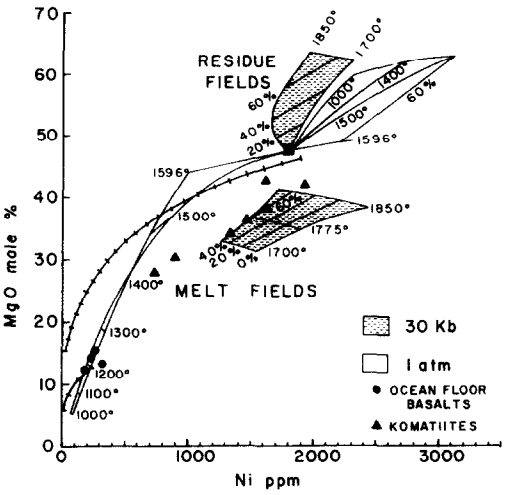

Figure 6. Ni-MgO diagram for batch melting of a pyrolite mantle with 1800 ppm Ni. The shaded fields show the results for K_d data at 30 Kb (BICKEL et al., 1977) and the unshaded fields for K_d data at one atmosphere (DAVIS and HART, 1977; ROEDER and EMSLIE, 1970). Curves for fractional crystallization of olivine at one atmosphere are shown with marks at intervals of 5% fractional crystallization of olivine. The residue and melt fields are contoured for temperature and fractions of batch melting. Selected komatiites and ocean floor basalts are also plotted.

et al. (1977) K_d's at one atmosphere for Ni are from DAVIS and HART (1977) who give $K_d = (124.13/MgO) - 0.897$, where MgO is in weight percent. K_d's at 30 Kb for Ni are based on a temperature dependence for K_d at one atmosphere given by DAVIS and HART (1977), which has been extrapolated to the appropriate temperatures for melting at 30 Kb. This extrapolation is probably valid based on data for Ni at 30 Kb reported by BICKLE et al. (1977). D_{Ni} for the pyrolite residue was calculated assuming

$$D_{Ni} = \left(\frac{C_s^{MgO}}{C_{ol}^{MgO}}\right)^2 K_{d_{Ni}}^{ol/L} \qquad (12)$$

The basis for this calculation is that C_s^{Ni}/C_{ol}^{Ni} is always smaller than C_s^{MgO}/C_{ol}^{MgO} and yet must vary from about 0.65 to 1.0. As the MgO ratio varies from about 0.8 to 1, the ratio of MgO in residue to MgO in olivine squared is probably a good approximation.

Fractional crystallization curves for olivine are drawn in Figure 6 with marks for 5% intervals of fractional crystallization. These were calculated concurrently with the fractional crystallization curves for olivine for MgO and FeO. Thus, because of the 0.1% steps for fractional crystallization it was possible to continuously change the K_d's for Ni as the temperature of the melt and the composition of the olivine and melt changed. Due to large K_d's for both Ni and MgO at lower temperatures, the subparallel curves for fractional crystallization show rapid depletion of Ni and MgO with small extents of fractional crystallization of olivine.

Use of appropriate MgO-Ni and MgO-FeO diagrams together for basaltic or mafic melts should allow a very good estimate of the temperature and extent of partial melting of a possible parent melt. It also places strong constraints on the extent of fractional crystallization or accumulation of olivine that a melt may have undergone.

Incompatible Element-MgO

A plot of MgO versus C_o/C_L for incompatible trace elements is shown in Figure 7. Plotted in this way, very small extents of partial melting plot near the MgO axis, and the value of C_o/C_L is equal to the extent of partial melting, F. The lines for constant extents of partial melting are vertical, since D for the incompatible element is zero. On this plot, crystal accumulation, fractional crystallization and increased melting with increasing temperature all show the same trends, i.e. MgO increases as C_o/C_L increases. Consequently, such plots have limited value for discriminating among such hypotheses. In particular, linear trends of mafic and ultramafic rocks on plots of MgO versus incompatible elements need not intersect the parent composition of the mantle as has been assumed by various workers.

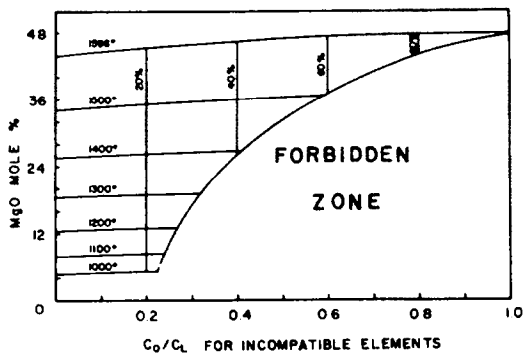

Figure 7. MgO - Incompatible element diagram for batch melting at one atmosphere. The MgO compositions are from Figure 2 for a mantle of pyrolite composition. The area to the right of the melt field is the forbidden zone for melts, which is determined by the maximum extents of partial melting at a given temperature determined from the MgO-FeO diagram. It can only be entered if the incompatible element concentration in the source is less than the assumed value for C_o or by continuous melting.

APPLICATIONS

In the following section we will use the MgO-FeO diagram to consider the petrogenesis of some ocean floor basalts, komatiites and ultramafic nodules. Particularly in the latter two cases, there is an insufficient amount of K_d data over a range of T,P and composition to make rigorous conclusions, but it is still possible to make some significant observations. The K_d's of ROEDER and EMSLIE (1970) are probably appropriate for considering the origin of ocean ridge basalts, because they were determined using an oceanic basalt at low pressure.

It is not known whether the measured ferric-ferrous ratio in a rock represents that ratio during partial melting or fractional crystallization. In general, it appears that the analyzed ferric iron content makes up 10% of the total iron in ocean ridge basalts, 15% in alkali basalts and 5% in komatiites and ultramafic nodules. These may well be maximum values for the ferric contents of melts due to dehydrogenation of evolving melts and oxidation under surface conditions.

Ocean Floor Basalts

MgO and FeO contents of some of the least differentiated basalt glasses from the ocean floor (FREY et al., 1974; BRYAN and MOORE, 1977) with $Mg/Mg + Fe^{2+}$ atomic ratios of about 0.70 are plotted in Figure 8. All these glasses lie on or below the 0% melting line at temperatures less than 1300°C, suggesting that they do not represent primary melts from a pyrolite mantle. Because crystallization would drive the melt to higher FeO contents, primary magmas from which the glasses could be derived must fall on the FeO poorer side of olivine fractionation lines through the data points. This restricts possible primary magmas for these ocean floor basalts, if the parent is pyrolite, to less than 21.5 mole% MgO (15.5 weight %) and 6.4 mole% FeO (8.2 weight %). The constraint on FeO is independent of the parent composition, because it relies on the position of the olivine fractionation line. The constraint on MgO abundances could be raised only if the parent composition contained less FeO than pyrolite. Thus, it appears that although least differentiated ocean floor basalts may not be primary, they have undergone at most 5-10% fractional crystallization. This conclusion is substantiated for these samples on the MgO-Ni diagram (Figure 6), as they plot near the field for primary melts.

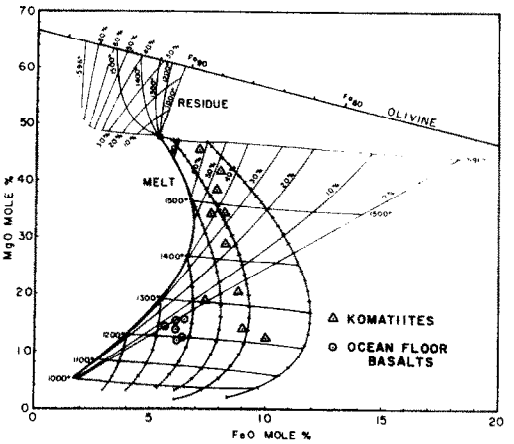

Figure 8, MgO-FeO diagram from Figure 5 with data from selected ocean floor basalts and Archean komatiites.

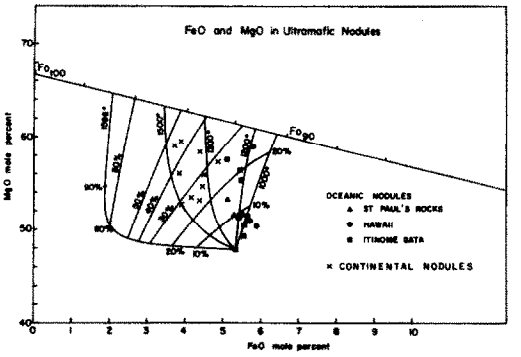

Figure 9. MgO-FeO diagram from Figure 2 with the data for selected ultramafic nodules (O'HARA et al., 1975; RHODES and DAWSON, 1975; KUNO, 1969; KUNO and AOKI, 1970; MELSON et al., 1967; TILLEY, 1947).

Komatiites

Figure 8 shows Archean komatiites ranging from 10 to 32 wt. % MgO (14 to 46 mole%) on the MgO-FeO plot. The data are from NESBITT and SUN (1976), BICKLE et al. (1975), NESBITT et al (1975), ARTH et al. (1977), ARNDT et al. (1977) and GREEN et al. (1975). Since komatiites may be high pressure melts, the temperatures shown in Figure 8 are not appropriate while the extents of melting probably are because of the small effect of pressure on the shape of the melt field.

The low magnesia content of rocks of the tholeiitic suite associated with komatiites (ARNDT et al., 1977) would be consistent with their derivation by lower extents of melting than komatiites. The iron-rich composition of these rocks relative to ocean ridge basalts suggests that if they were derived from pyrolite, then the partial melting took place at higher pressures and temperatures than for more recent tholeiites.

GREEN et al. (1975) reported experiments on one of the most magnesian komatiites (44 mole% MgO) and found only olivine on the liquidus. SUN and NESBITT (1977) have taken this and other data to conclude that komatiites are derived by 60-80% partial melting of the mantle leaving only olivine of Fo_{92} in the residue. If this is true, the trend of the data in the MgO-FeO plot shows that the parent compositions for the unmelted mantle would have had to be significantly more FeO-rich than pyrolite. Alternatively, it may be that 60-80% melting is not necessary to form komatiites. Based on the positions of the data on the MgO-FeO diagram, most could be derived by 30-50% melting, with the most magnesian by less than 70% melting. Furthermore, it appears that both olivine and pyroxene could be residual minerals for all komatiites.

The above arguments apply to batch melting. For continuous melting of pyrolite, the most magnesian komatiites could be derived by 25 to 60% melting depending on the proportion of melt continuously removed from the residue. Continuous melting would also account for the low CaO, Al_2O_3 and incompatible element abundances and the depleted REE patterns in the most magnesian komatiites. This is because continuous melting can progressively deplete the less compatible elements compared to the more compatible elements in melts relative to the original parent.

Untramafic Nodules

If the parent composition is known, the MgO and FeO contents of ultramafic nodules representing residues of batch melting can give the temperature and extent of melting at the time a mafic or basic liquid was separated from the nodule. Because of the pressure dependence of the K_d's, the temperatures given in Figure 9 are minimum while the extents of melting may be approximately correct (compare with Figure 4). Nodules are preferable to basalts for obtaining information on the conditions of melting, in that there is no uncertainty with respect to the extent of fractional crystallization. However, they have the disadvantage that they may contain resorbed residual melt, which would give the residue a composition closer to that of the parent and suggest lower extents of melting.

Figure 9 shows the MgO and FeO contents of St. Paul's Rock (MELSON et al., 1967; TILLEY, 1947) and of nodules from basalts from Hawaii (KUNO, 1969) and Itinomegata (KUNO and AOKI, 1970). All compositions have been recalculated as volatile free and Fe_2O_3 has been chosen arbitrarily as 4% of total iron. The data points fall in a field trending from a composition slightly more iron rich than pyrolite almost up to the composition of pure olivine. These nodules are consistent with extraction of a tholeiite derived by less than 30% melting at temperatures around 1300° from a mantle with MgO and FeO contents similar to pyrolite.

Figure 9 also shows nodules from kimberlites (KUNO and AOKI, 1970; O'HARA et al., 1975); and the Lashaine volcano (RHODES and DAWSON, 1975). These nodules, which group together, are poorer in iron than the nodules mentioned above. If they are derived from a parent similar to pyrolite, they reflect up to 50% melting at high temperatures and pressures. Alternatively, they may reflect continuous melting of more limited extents. They are appropriate residual compositions for melts of the komatiite suite derived from a pyrolite mantle.

Clearly the two sets of nodules represent different melting conditions, but the initial parent compositions may have been similar. Since the effect of pressure will be to move residual compositions to lower FeO at a given MgO, the continental nodules may reflect high pressure, high temperature melting, while those from basalts may represent lower pressure, lower temperature melting. These conditions are probably reflecting the respective tectonic environments, and the heterogeneity in the MgO and FeO contents of the nodules need not result from heterogeneity in the original mantle.

CONCLUDING REMARKS

We have presented a method for the quantitative modelling of major elements, which combines the use of major element K_d's for individual elements with the theoretical equations for partial melting and fractional crystallization which have been used for modelling trace elements. In contrast to trace elements, modelling major elements requires monitoring the composition of the minerals involved. Thus, simply using K_d's for major elements in the trace element equations will lead to erroneous results. The stoichiometric constraints of the minerals make modelling more difficult, but give additional information regarding the change in the composition of the minerals as melting or crystallization proceeds. As an example we have chosen MgO and FeO in the mantle-melt system. It should be possible to apply the same methods to other elements. Such modelling will require knowledge of the variation of the K_d's for major elements as a function of T,P and composition and these data are presently not available.

We emphasize finally that for precise petrogenetic modelling, K_d data should be given in mole fractions. K_d's for both major and trace elements given as weight fractions vary with the atomic weight of the phases in the system, which can lead to significant errors over a range of compositions such as basalt to komatiite. In addition, mole fractions are needed in order to relate K_d's to thermodynamic parameters.

Acknowledgments

We wish to acknowledge the discussions with and encouragement from A.E. Bence, J. Bender, and D.H. Lindsley. The critical reviews of D.C. Presnall and P.L. Roeder led to a significant improvement in the manuscript. Financial support was provided by National Science Foundation Grants No. EAR 76-13354 (Geochemistry) and DES 74-22511 (Submarine Geology Section).

REFERENCES

ARNDT N.T., NALDRETT A.J. and PYKE D.R. (1977) Komatiitic and iron-rich tholeiitic lavas of Munro Township, Northeast Ontario. J. Petrol. 18, 319-369.

ARTH J.G., ARNDT N.T. and NALDRETT A.J. (1977) Genesis of Archean komatiites from Munro Township, Ontario: trace element evidence. Geology 5, 590-594.

BICKLE M.J., FORD C.E. and NISBET E.G. (1977) The petrogenesis of peridotitic komatiites: evidence from high-pressure melting experiments. Earth Planet. Sci. Lett. 37, 97-106.

BICKLE M.J., MARTIN A. and NISBET E.G. (1975) Basaltic and periodotitic komatiites and stromatolites above a basal unconformity in the Belingue greenstone belt, Rhodesia. Earth Planet. Sci. Lett. 27, 155-162.

BOWEN N.L. (1928) The evolution of igneous rocks. Princeton University Press, 334 p.

BRYAN W.B. and MOORE J.G. (1977) Compositional variations of young basalts in the Mid-Atlantic ridge rift valley near 36° 49'N. Geol. Soc. Am. Bull. 88, 556-570.

DAVIS K.E. and HART S.R. (1977) Partitioning of nickel between olivine and silicate liquid. (abstr.) In papers presented to the International Conference on Experimental Trace Element Geochemistry, 16-17.

FREY F.A., BRYAN W.B. and THOMPSON G. (1974) Atlantic Ocean floor: geochemistry and petrology of basalts from legs 2 and 3 of the Deep-Sea Drilling Project. J. Geophys. Res. 79, 5507-5527.

GAST P.W. (1968) Trace element fractionation and origin of tholeiitic and alkaline magma types. Geochim. Cosmochim. Acta 32, 1057-1086.

GREEN D.H. (1976) Experimental petrology in Australia--a review. Earth Sci. Rev. 12, 99-138.

GREEN D.H., NICHOLLS I.A., VILJOEN M.J. and VILJOEN R.P. (1975) Experimental demonstration of the existence of peridotitic liquids in earliest Archean magmatism. Geology 3, 11-14.

IRVINE T.N. (1974) Petrology of the Duke Island ultramafic complex, Southeastern Alaska. Geol. Soc. Amer. Memoir 138, 240 p.

KUNO H. and AOKI K.I. (1970) Chemistry of ultramafic nodules and their bearing on the origin of basaltic magmas. Phys. Earth Planet. Interiors 3, 273-301.

LANGMUIR C.H., BENDER J.B., BENCE A.E., HANSON G.N. and TAYLOR S.R. (1977) Petrogenesis of basalts from the Famous area: Mid-Atlantic Ridge. Earth Planet. Sci. Lett. 36, 133-156.
LANGMUIR C.H. and HANSON G.N. (1977) Dynamic melting of mantle. (abstr.) In papers presented to the International Conference on Experimental Trace Element Geochemistry, 68-70.
LONGHI J., WALKER O. and HAYS J.F. (in press) The distribution of Fe and Mg between olivine and lunar basaltic liquids. Geochim. Cosmochim. Acta.
MELSON W.G., JAROSEWICH E., BOWEN V.T. and THOMPSON G. (1967) St. Peter and St. Paul Rocks: a high temperature, mantle-derived intrusion. Science 155, 1532-1535.
MORSE S.A. (1976) The lever rule with fractional crystallization and fusion. Amer. J. Sci. 276, 330-346.
MYSEN B.O. and KUSHIRO I. (1977) Compositional variations of coexisting phases with degree of melting of peridotite in the upper mantle. Amer. Mineral. 62, 843-856.
NESBITT R.W. and SUN S.S. (1976) Geochemistry of Archean spinifex-textured peridotites and magnesian and low-magnesian tholeiites. Earth Planet. Sci. Lett. 31, 433-453.
NEUMANN H., MEAD J. and VITALIANO C.J. (1954) Trace element variation during fractional crystallization as calculated from the distribution law. Geochim. Cosmochim Acta 6, 90-99.
O'HARA M.J., SAUNDERS M.J. and MERCY E.L.P. (1975) Garnet-peridotite, primary ultra-basic magma and eclogite; interpretation of upper mantle processes in kimberlite. Phys. Chem. of the Earth 9, 571-604.
PRESNALL D.C. (1969) The geometric analysis of partial fusion. Am. J. Sci. 267, 1178-1194.
RAHEIM A. and GREEN D.H. (1974) Experimental determination of the temperature and pressure dependence of the Fe-Mg partition coefficient for coexisting garnet and clinopyroxene. Contrib. Mineral. Petrol. 48, 179-203.
RHODES J.M. and DAWSON J.B. (1975) Major and trace element chemistry of peridotite inclusions from the Lashaire volcano, Tanzania. Phys. Chem. of the Earth 9, 545-550.
RINGWOOD A.E. (1975) Composition and Petrology of the Earth's Mantle. McGraw-Hill, New York, 613 p.
ROEDER P.L. (1974) Activity of iron and olivine solubility in basaltic liquids. Earth Planet. Sci. Lett. 23, 397-410.
ROEDER P.L. (1975) Thermodynamics of element distribution in experimental mafic silicate-liquid systems. Fortschr. Miner. 52. Special issue (I.M.A. Ninth General Meeting) 61-73.
ROEDER P.L. and EMSLIE R.F. (1970) Olivine-liquid equilibrium. Contrib. Mineral. Petrol. 29, 275-289.
SCHILLING J.G. (1966) Rare earth fractionation in Hawaiian volcanic rocks. Ph.D. thesis, Mass. Inst. of Technology.
SHAW D.M. (1970) Trace element fractionation during anatexis. Geochim. Cosmochim. Acta 34, 237-243.
SUN S.S. and HANSON G.N. (1975) Origin of Ross Island basanitoids and limitations upon the heterogeneity of mantle sources for alkali basalts and nephelinites. Contrib. Mineral. Petrol. 52 77-106.
SUN S.S. and NESBITT R.W. (in press) Petrogenesis of Archean ultrabasic and basic volcanics: evidence from rare earth elements. Contrib. Mineral. Petrol.
TILLEY C.E. (1947) The dunite-mylonites of St. Paul's rocks (Atlantic). Am. J. Sci. 245, 483-491.
WRIGHT T.L. and DOHERTY D.C. (1970) A linear programming and least-squares computer method for solving petrologic mixing problems. Bull Geol. Soc. Amer. 81, 1995-2008.

Appendix 1

As an example of how the compositions of melts between minimum and maximum melting are calculated, detailed calculations for determining MgO and FeO for 30% melting (F=0.3) of pyrolite at 1400°C for the MgO-FeO plot in Figure 2 are given here. Maximum melting at 1400°C is 41%.

For pyrolite, the parent composition, C_o, is:

MgO = 47.8 mole% FeO = 5.35 mole%

From equations (6) and (7)

$$K_{d_{MgO}}^{ol/L} = 2.32 \qquad K_{d_{FeO}}^{ol/L} = 0.688$$

It is possible to start with any D, but quicker to start with a D interpolated between the minimum and maximum extents of melting. D's for the maximum extent of melting at 1400°C for MgO and FeO are $K_d^{ol/L}$ i.e. 2.32 and 0.688 respectively. At the minimum extent of melting for D's for MgO and FeO are 1.86 and 0.513 respectively. We will select a D about three-fourths way between these values i.e.

$$D_{MgO} = 2.20 \qquad D_{FeO} = 0.65$$

A melt is then calculated using equation (3)

$$C_L = \frac{C_o}{D(1-F) + F}$$

$$C_L^{MgO} = (47.8)/((2.20)(0.7) + 0.3) = 25.98\%$$

$$C_L^{FeO} = (5.35)/((0.65)(0.7) + 0.3) = 6.83\%$$

A residue is then calculated using equation (1):

$$C_s = DC_L$$

$$C_s^{MgO} = (2.20)(25.98) = 57.16\%$$

$$C_s^{FeO} = (0.65)(6.83) = 4.44\%$$

This residue is then plotted on the MgO-FeO diagram (Figure A-1). Figure A-1 contains the lines of olivine, orthopyroxene and clinopyroxene compositions, and several sets of coexisting minerals from ultramafic nodules. From the position of the residue on the plot (pt. A in Figure A-1), the composition of the olivine in the residue can be estimated as Fo_{93}, i.e.

$$C_{ol}^{MgO} = 62.0\% \qquad C_{ol}^{FeO} = 4.67\%$$

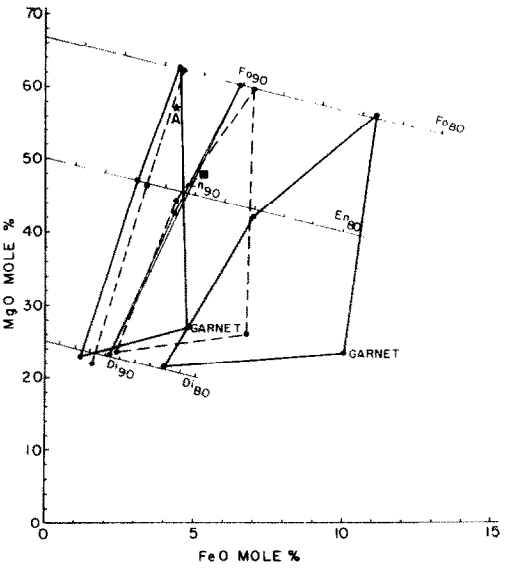

Figure A-1. Plot of MgO-FeO with lines of olivine, orthopyroxene and clinopyroxene compositions. Mineral data from ultramafic nodules are also plotted. The composition of an olivine in any total solid composition near the olivine line can be estimated using the mineral data. Note, for example that for the two nodules with olivine near Fo_{90}, although the olivine/orthopyroxene K_d's differ, estimated olivines for the same bulk compositions would be very similar. We suggest that olivine compositions may be estimated to within $Fo_{0.5}$. Point A is the calculated residue referred to in the text. The solid square is the composition of pyrolite.

New D's are then calculated using equation (5)

$$D_{MgO} = \frac{C_s^{MgO}}{C_{ol}^{MgO}} K_d^{ol/L} = \frac{57.16}{62.0} (2.32) = 2.14$$

$$D_{FeO} = \frac{4.44}{4.67} (0.69) = 0.657$$

These D's are then used in equation (3)

$$C_L^{MgO} = 26.59\%$$

$$C_L^{FeO} = 7.05\%$$

A new residue is calculated using equation (1)

$$C_s^{MgO} = 56.90\% \qquad C_s^{FeO} = 4.62\%$$

The residue is plotted on the MgO-FeO diagram and a new olivine estimated, $Fo_{92.7}$ i.e.

$$C_{ol}^{MgO} = 61.8\% \qquad C_{ol}^{FeO} = 4.87\%$$

Then, using the same methods as above:

$$D_{MgO} = 2.14 \qquad D_{FeO} = 0.653 \qquad C_s^{MgO} = 56.99\%$$

$$C_L^{MgO} = 26.63 \qquad C_{ol}^{MgO} = 61.8\% \qquad C_s^{FeO} = 4.62\%$$

$$C_L^{FeO} = 7.07 \qquad C_{ol}^{FeO} = 4.87\%$$

Recalculating new D's leads to identical results as the last iteration, so the solution has converged. We can now check the results by making sure the liquid is in equilibrium with olivine by the relation:

$$C_{ol} = C_L K_d^{ol/L}$$

This yields

$$C_{ol}^{MgO} = 61.8\% \qquad C_{ol}^{FeO} = 4.87\%$$

which sums to 66.67% showing that stoichiometrically the mineral is olivine. Since this olivine is the same as the estimated olivine the results are internally consistent and we have arrived at the unique solution with olivine, residue and melt all in equilibrium with one another.

Note Added in Proof

The K_d's used in this paper were calculated using the equations of ROEDER and EMSLIE (1970). It has been brought to our attention by M. Fisk (oral communication, 1978) that their K_d's were calculated using the mole% of oxide (molecular weight is based on SiO_2, Al_2O_3, Na_2O etc.). Whereas we have used mole% of cations (molecular weight is based on SiO_2, $AlO_{1.5}$, $NaO_{0.5}$ etc.). This means that the K_d's we have used are about 10% lower than those of ROEDER and EMSLIE (1970). The values for K_d used in this paper are very similar to those determined by BENDER, HODGES and BENCE (in prep.) on ocean floor basalts from the FAMOUS area.